

Call for Papers

SPIE International Symposium

Medical Imaging

12–17 February 2005

Town and Country Hotel
San Diego, California USA

Conferences • Courses • Exhibition

Inviting papers on:

**Visualization, Image-Guided Procedures,
and Display**

Physics of Medical Imaging

**Physiology, Function, and Structure from
Medical Images**

Image Processing

PACS and Imaging Informatics

**Image Perception, Observer Performance,
and Technology Assessment**

Ultrasonic Imaging and Signal Processing

Submit your abstract today!

*Publish your work—in SPIE's
Digital Library and in print!*

 The International Society
for Optical Engineering

Unbiased Rigid Registration using Transfer Functions

Dieter A. Hahn^a, Joachim Hornegger^a, W. Bautz^b, T. Kuwert^c and W. Römer^c

^aFriedrich-Alexander University (FAU) - Pattern Recognition, Martensstr. 3, 91058 Erlangen, Germany

^bFAU, Institute of Radiology, Maximiliansplatz 1, 91054 Erlangen, Germany

^cFAU, Clinic of Nuclear Medicine, Krankenhausstr. 12, 91054 Erlangen, Germany

ABSTRACT

The evaluation of tumor growth as regression under therapy is an important clinical issue. Rigid registration of sequentially acquired 3D-images has proven its value for this purpose. Existing approaches to rigid image registration use the whole volume for the estimation of the rigid transform. Non-rigid soft tissue deformation, however, will imply a bias to the registration result, because local deformations cannot be modeled by rigid transforms. Anatomical substructures, like bones or teeth, are not affected by these deformations, but follow a rigid transform. This important observation is incorporated in the proposed registration algorithm. The selection of anatomical substructure is done by manual interaction of medical experts adjusting the transfer function of the volume rendering software. The parameters of the transfer function are used to identify the voxels that are considered for registration. A rigid transform is estimated by a quaternion gradient descent algorithm based on the intensity values of the specified tissue classes. Commonly used voxel intensity measures are adjusted to the modified registration algorithm. The contribution describes the mathematical framework of the proposed registration method and its implementation in a commercial software package. The experimental evaluation includes the discussion of different similarity measures, the comparison of the proposed method to established rigid registration techniques and the evaluation of the efficiency of the new method. We conclude with the discussion of potential medical applications of the proposed registration algorithm.

Keywords: Mono-modal Registration, Rigid Registration, Voxel Intensity, Similarity Measure, Transfer Function, Unbiased Estimation, Gradient Descent, Optimization

1. INTRODUCTION

Virtually all registration techniques that make use of voxel similarity measures have been successfully applied to single subject serial studies and there exist several surveys of rigid medical image registration, i.e. in Brown,¹ Elsen et al.,² Hajnal et al.,³ Hill et al.,⁴ Maintz et al.⁵ or Woods et al.⁶ Our approach provides an improvement in regard to the registration of images that feature significant non-rigid soft tissue deformations in anatomical regions of interest. Especially in computed tomography (CT) and magnetic resonance imaging (MRI), tissue can be identified by its intensity value in the according grey value image. Thus different classes of tissue can be quantified by appropriate transfer functions. The modification of given voxel similarity measures allows to consider only specified tissue for registration. We will show an implementation and integration of the unbiased rigid registration using transfer functions into a clinical environment and present the improvements in comparison to commonly used approaches which administer the whole image information. This application can be used to identify and visualize longitudinal dependent tissue deformations in serially acquired CT images before (e.g. the lymphoma patient seen in figure (fig.) 1(a)) and after the treatment (fig. 1(b)). The checkerboard fusion image (CFI) clearly demonstrates the significant impact the large tissue deformation has on the standard registration approach, such as the inadequate alignment of the cranial bones in fig. 1(c). In contrast, the CFI in fig. 1(d) shows the unbiased rigid registration using a transfer function for osseous structure resulting in an enhanced alignment of the images. Furthermore, as the results of the rigid registration can be used either independently or in combination, the presented approach offers advanced starting points for further computations, such as non-rigid registration techniques.

Contact author:

E-mail: Joachim.Hornegger@informatik.uni-erlangen.de, Phone: +49 9131 85-27775

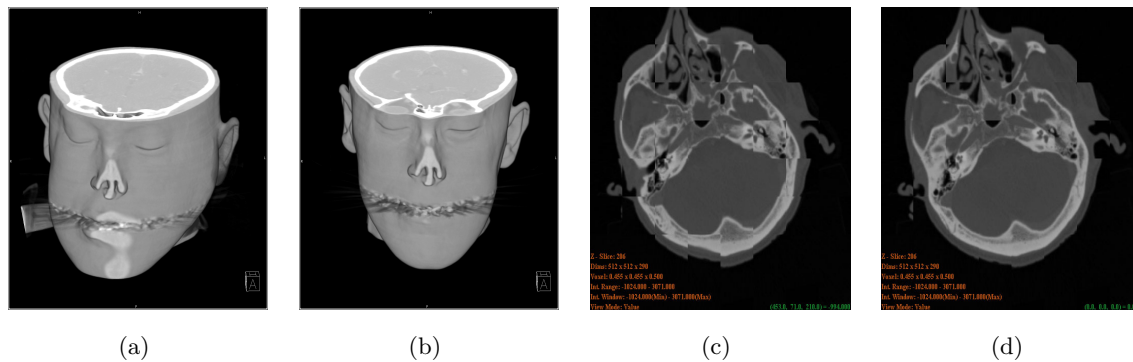


Figure 1. Significant non-rigid tissue deformation in two slices of sequentially acquired 3D CT images in the lymphoma area before 1(a) and as a result of the treatment 1(b). The CFI slices of the rigidly registered 3D image using the whole image information 1(c) and the presented approach 1(d).

Scale Space Index	Image Scaling Factor	Gaussian Variance	Cluster Field Size	Cluster Size
0	1/16	16	1x1x1	32
1	1/8	8	1x1x1	16
2	1/4	4	2x2x2	16
3	1/2	2	2x2x2	16
4	1	—	2x2x2	8

Table 1. Parameter settings for images up to $512 \times 512 \times 512$ voxels with the according cubical cluster sizes (in voxels as well). Scale space index 4 corresponds to the last registration using the original un-scaled image resolution.

2. METHODS

The algorithm mainly consists of three parts: the registration preprocessing, the optimization that implies the computation of the modified similarity measures and the registration post-processing. In our approach, a hierarchical scale space representation of the images is employed, in order to reduce computation time as well as to increase the accuracy of the registration result.

2.1. Registration Preprocessing

Scaling and Gaussian filtering are applied to images, allowing the computation of approximated rigid transforms \mathcal{T}_i in the prior stages, with $i \in \{1, \dots, N\}$ being the number of the according scale space. In order to receive the final transform \mathcal{T} , the registration is applied to the high resolution images with the final scale space approximation \mathcal{T}_N as input transform. The whole process can be further accelerated by making use of a clustering approach to reduce the large amount of computation needed for the intensity similarity measures. We have adopted the approach of Althof⁷ to 3D images and with an adequate clustering, results can be acquired faster without losing their accuracy. A typical clustering configuration for the registration is shown in table 1. The configuration can be changed without compilation of the application, thus the program is scalable to the growing computational power of processing units. As the registration transform gets more accurate with higher scale space level, i.e. with better image resolution, the cluster sizes can be down-scaled, which results in an additional performance gain compared to fixed cluster sizes.

2.2. Optimization

We have implemented and modified several commonly used similarity measures in order to support transfer function values at the voxel positions $TF(voxel)$, see equation (eq.) 1. If the voxel position is outside the overlap domain (see also appendix A) a default intensity value can be specified that is neutral to the registration, e.g. the minimal image intensity. The physician can interactively define the intensities through choosing an appropriate

piecewise linear transfer function within the medical application. Thus the physician can interactively adapt the transfer function and precisely choose the tissue that has to be registered.

$$t(\text{voxel}) = \begin{cases} TF(\text{voxel}) & : \text{ voxel} \in \Omega, \text{ with } \Omega \text{ being the overlap of the images} \\ I_{\text{default}} & : \text{ otherwise, where } I_{\text{default}} \text{ is a predefined intensity value} \end{cases} \quad (1)$$

Eq. 1 can be adapted to inverse, concatenated ranges as well as to non-linear transfer function values. We have implemented and tested several standard similarity measures. Among them are the widely used intra modality measures sum of squared and absolute differences, the mutual and normalized mutual information, correlation, cross correlation, normalized cross correlation, the ratio image uniformity and the histogram of differences. See section A for the mathematical definition of the implemented measures.

The optimization of the transform \mathcal{T} on the basis of image intensity similarity measures is performed with a quaternion gradient descent algorithm on a 7 dimensional (7-D) parameter space $P \subset R^7$. Each parameter set specifies a position p in P . In order to avoid the search for the best step-size into the descent direction as practiced in some versions of the algorithm, like the steepest gradient descent (e.g. in Venkataraman⁸) or in derivatives which use less restricting step-size criteria (e.g. Armijo⁹ criterion), we developed an approach that approximates the step size based on the angle between the last and the current gradient. The mechanism acts like a castigator on the step length if the angle is large and like a benefactor if the angle is small. It can be expressed using a weight function w (eq. 2) that is directly proportional to the scalar product of the function gradients at the k th and the $k-1$ th parameter set. In our empirical experiments, we achieved good results using the weight function given in eq. 3.

$$w(\nabla f(p_k), \nabla f(p_{k-1})) \quad \text{where } \nabla \text{ being the 7-D gradient,} \quad (2)$$

$$w(x, y) = \frac{1}{2} \frac{x^T \cdot y}{\sqrt{\|x\| \cdot \|y\|}} + 1 \quad \|\dots\| \text{ being the Euclidean norm} \quad (3)$$

Computation time can be saved by approximating a descent step size that is not necessarily the steepest descent but lets the algorithm firmly converge towards the optimum. Therefore less evaluations of the similarity measure are needed, which is the most expensive part regarding the computational effort. The parameter search process can then be formulated as the iterative update of the position p from iteration k to $k+1$, see eq. 4. The compact version of the optimization method is given in algorithm 1.

$$p_{k+1} = p_k - \lambda \cdot \nabla f(p_k) \cdot w(\nabla f(p_k), \nabla f(p_{k-1})) \quad (4)$$

Algorithm 1 Gradient-Based Optimization

Require: $\epsilon_f \geq 0; \lambda \neq 0; \delta > 1; n_{max} > 0$

- 1: $k \leftarrow 1$
 - 2: initialize p_0, p_1
 - 3: **while** $\|\nabla f(p_k)\| > \epsilon_f$ and $k < n_{max}$ **do**
 - 4: approximate the step size factor: $w^* \leftarrow w(\nabla f(p_k), \nabla f(p_{k-1}))$
 - 5: **while** $f(p_k - \lambda \cdot \nabla f(p_k) \cdot w^*)$ worse than $f(p_k)$ **do**
 - 6: $w^* \leftarrow \frac{w^*}{\delta}$
 - 7: **end while**
 - 8: $p_k \leftarrow p_k - \lambda \cdot \nabla f(p_k) \cdot w^*$
 - 9: $k \leftarrow k + 1$
 - 10: **end while**
-

2.3. Registration Post-processing

Given the optimized parameter position specified by the final transform T the image B is re-sampled and interpolated to the new spatial position. Several techniques of image combination can then be applied to visualize the registration result. The fused images can be visualized with advanced, in medical systems already available, volume rendering graphics hardware that is capable of rendering at least two high resolution images at the same time. The images shown in this article were created by checkerboard fusion of the fixed and the transformed moving image and by image subtraction. In order to evaluate our implementation in clinical practice, the algorithm has been integrated into a commercial software package¹⁰ that is commonly used in hospitals and has a high recognition value for physicians. One of the main goals of the project was the formation of a robust, user-friendly applicable and fast enough version of the algorithm to persist in the clinical environment (fig. 2).

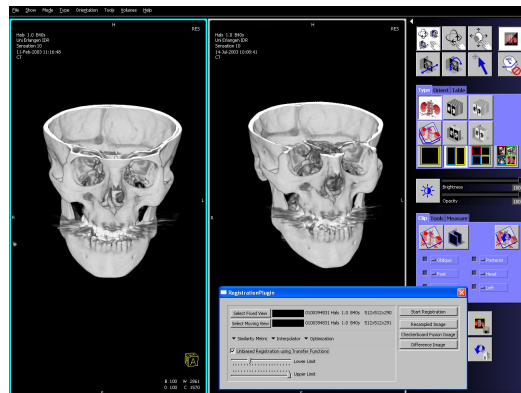


Figure 2. The registration plug-in that works on two input images and that supports eight different similarity measures, three interpolation strategies, the common rigid body registration approach and the application of transfer functions for the unbiased rigid registration.

3. RESULTS

In order to analyze the accuracy of the registration high resolution 3D medical data sets (512x512x200 voxels) were transformed with known parameter sets and used as input data in order to compare the proposed method to established rigid registration techniques. As the position of the patient who will be scanned sequentially with a medical acquisition system is limited to certain ranges, estimated parameters were chosen for the transforms. It is shown that the results of the proposed approach are equivalent to those of well established techniques for artificial test images without non-rigid deformations and even better for sequentially acquired real data sets with non-rigid deformations. In practice, sequential images are likely to feature non-rigid tissue deformations (see fig. 1) which imply a bias to established algorithms. The presented technique has been applied to such sequentially acquired CT images of tumor patients. The evaluation of the registration results in this case is no longer possible using only the pure values of the similarity measures as the registration of certain tissue classes is likely to produce different overall image similarities. Visual assessment was done regarding the matching of the tissue structure contours using the CFI technique and difference imaging. The amount of information contributed by the registered tissue class to the fused image is minimal as these structures diminish in the difference image with the degree of alignment. This can be seen in the images of fig. 3 where the teeth are misaligned in the common approach due to the featured non-rigid soft tissue deformation resulting from therapy. The overall alignment could be improved by our unbiased registration using a transfer function that excludes the mentioned soft tissue.

In scans featuring non-rigid deformations, like intestinal motion in fig. 6 or motion of the respiratory system and the heart in fig. 4(a), the application of rigid registration is limited. However, it can be applied to those structures which are not affected by these deformations. Compared to the common approach the registration of the spine alone, as well as the registration of osseous structures improved the results in the mentioned data sets. A more detailed view of a region of interest is given in fig. 5.

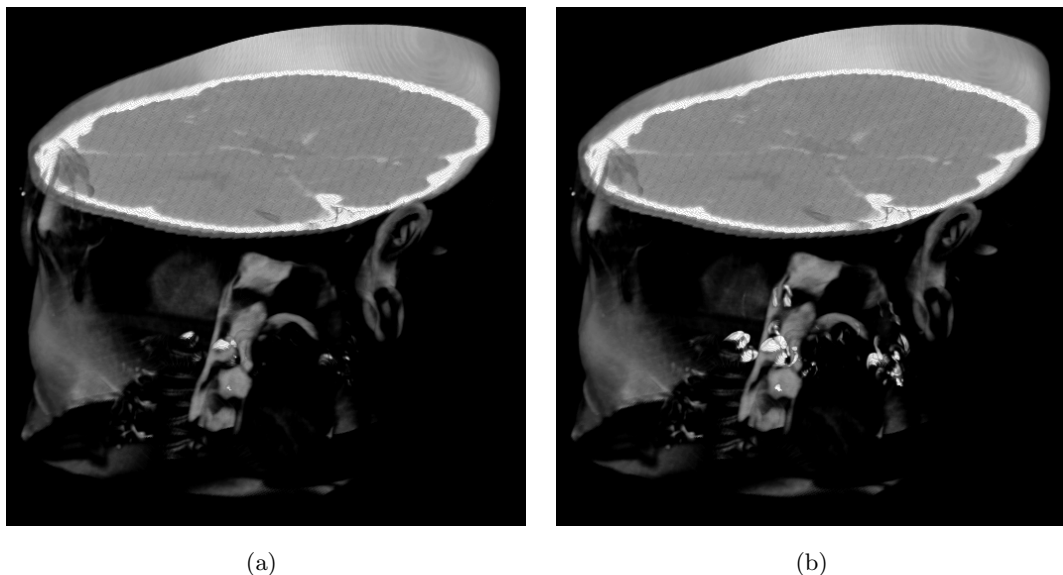


Figure 3. Fig. 3(a) shows a better overall alignment due to the usage of a transfer function for the presented approach that excludes the soft tissue from the registration process. In contrast, the difference image between the fixed and the registered re-sampled moving image resulting from the common approach can be seen in fig. 3(b).

The efficiency of the proposed method was rated on basis of the computation time with respect to the implemented standard approach. Applying the parameter set of table 1, the registration was performed with an accuracy of $1e-8$ for the parameter positions and a maximum of 100 iterations for each of the pyramidal scale space steps. The resulting computation times for the different methods used with various similarity measures are given in table 2. The speed was evaluated on a 2.0 GHz AMD mono processor system with 1.3 GByte main memory.

Method	SAD	SSD	CC	RIU	EHD	MI	NMI
Common [s]	204.94	163.73	140.40	55.77	45.93	76.11	49.49
Unbiased [s]	136.37	175.43	97.77	37.37	26.39	76.17	40.90

Table 2. The table shows the computation times of the algorithms in seconds for the different similarity measures. The times incorporate the optimization and the resampling of the images at each scale space step, i.e. from the start to the approximated rigid transform.

4. SUMMARY

This article presents a new way of improving rigid registrations for sequential medical images featuring significant non-rigid deformations. The negative side effects of such deformations can be significantly attenuated without computational extra costs through modifying commonly used similarity measures. The physician can interactively affect the registration by defining an appropriate transfer function for anatomical structures that are not affected by non-rigid deformations in order to register sequential images more accurately. This approach has been successfully applied to high resolution CT images of lymphoma patients. Several well known voxel intensity-based similarity measures have been adapted to support the unbiased registration using transfer functions. In comparison to well established algorithms our approach shows a better performance on sequentially acquired images exhibiting non-rigid tissue deformations. For the assessment of the registration results by medical experts several visualization techniques can be applied. However, a wider field of medical applications can be improved:

In combined approaches, where a rigid body transform is used to approximate a starting value for a subsequent non-rigid registration, the result could be achieved in a faster and more accurate way. Given the fact that in MRI, the contrast of bones usually is very bad, CT-MRI inter-modality registration could be improved by selecting tissue classes in the CT images that are also visible in the MR images and vice versa, thus increasing the accuracy of the result. In DSA, the contrast agent is only visible in the fill image and therefore could be masked out by setting an appropriate thresholding for the registration. Medical applicability is given for instance not only in nuclear medicine, where tumor changes are visualized, but also in Ear Nose and Throat medicine or neurology. The integration of the algorithm into a clinical environment allows the registration with user defined transfer functions and the visualization of the registration results in a commercial volume renderer. The future work concentrates on the acceleration and implementation of the described registration approach either by making use of dedicated central processing unit instructions which operate on multiple data elements simultaneously or by parallelizing and porting time critical parts of the algorithm onto graphics hardware.

5. ACKNOWLEDGEMENTS

The authors gratefully acknowledge the financial support by the Deutsche Forschungsgesellschaft (DFG) through grant SFB 603, TP C10, and ELAN-Fonds of the Clinical Faculty of the FAU (AZ:04.03.10.1). We also acknowledge Siemens Medical Solutions and HipGraphics Inc. for supplying the framework FTK (Fusion ToolKit) and InSpace3D licenses and support. The authors thank Gabriele Wolz for the investigation on appropriate sequential CT studies of tumor patients and the review of the article.

APPENDIX A. DEFINITIONS OF SIMILARITY MEASURES

In the notation used by Hajnal et al.³ the registration transform T represents the spatial mapping from the coordinate system of image A to the corresponding coordinate system of the sequential image B , with $x_A, x_B \in R^3$ being the voxel coordinates of image A and image B respectively (eq. 5) and contained within the image domains Ω_A and Ω_B . As T maps only between coordinates, however, an enhanced transform \mathcal{T} has to be introduced to additionally interpolate the intensity values at arbitrary coordinate positions.

$$T : x_A \mapsto x_B \Leftrightarrow T^{-1}(x_B) = x_A, \text{ where } x_A \in \Omega_A \text{ and } x_B \in \Omega_B \quad (5)$$

$$\Omega_{A,B}^T = \Omega = \{x_B \in \Omega_B | T^{-1}(x_B) \in \Omega_A\} \quad (6)$$

\mathcal{T} is only defined for the overlapping region of the images, the overlap domain Ω (eq. 6). $A(x_A)$ embodies the image value at position x_A of image A whereas $B^T(x_A)$ stands for the (interpolated) image intensity value of the transformed point x_A in image B .

Cross correlation (C, eq. 7), correlation coefficient (CC, eq. 8) and the normalized cross correlation (NCC, eq. 9) all show good results if the intensities of the images are linearly related. This class of measures has been applied in digital image processing since the seventies and can be used for digital subtraction angiography (DSA) as well, see Meijering¹¹ or Hajnal et al.³

$$C = \sum_{x_A \in \Omega_{A,B}^T} A(x_A) B^T(x_A) \quad (7)$$

$$CC = \frac{\sum_{x_A \in \Omega_{A,B}^T} (A(x_A) - \bar{A})(B^T(x_A) - \bar{B})}{\sqrt{\sum_{x_A \in \Omega_{A,B}^T} (A(x_A) - \bar{A})^2 \sum_{x_A \in \Omega_{A,B}^T} (B^T(x_A) - \bar{B})^2}} \quad (8)$$

$$NCC = \frac{\sum_{x_A \in \Omega_{A,B}^T} A(x_A) B^T(x_A)}{\sqrt{\sum_{x_A \in \Omega_{A,B}^T} A^2(x_A) \sum_{x_A \in \Omega_{A,B}^T} (B^T(x_A))^2}} \quad (9)$$

The sum of the absolute differences (SAD, eq. 10) and the sum of squared differences (SSD, eq. 11) are applied directly on the image intensity values and can therefore be used only in intra-modality image registration. In the case of images containing small amounts of voxels that show significant intensity differences, i.e. CT images with metal inlays, SSD is very sensitive. The effect of those outliers on the registration result can be reduced by applying SAD instead.

$$SAD = \frac{1}{N} \sum_{x_A \in \Omega_{A,B}^T} |A(x_A) - B^T(x_A)| \quad (10)$$

$$SSD = \frac{1}{N} \sum_{x_A \in \Omega_{A,B}^T} |A(x_A) - B^T(x_A)|^2 \quad (11)$$

The ratio image (R, eq. 12) is the basis for the ratio image uniformity (RIU, eq. 14) that can also be thought of as a measure for the normalized standard deviation of intensity values in R. Although the method originally has been applied to serial PET and serial MR registration it has been successfully applied to the proposed approach.

$$R(x_A) = \frac{A|_{\Omega_{A,B}^T}(x_A)}{B^T|_{\Omega_{A,B}^T}(x_A)} \quad (12)$$

$$\bar{R} = \frac{1}{N} \sum_{x_A \in \Omega_{A,B}^T} R(x_A) \quad (13)$$

$$RIU = \frac{\sqrt{\frac{1}{N} \sum_{x_A \in \Omega_{A,B}^T} (R(x_A) - \bar{R})^2}}{\bar{R}} \quad (14)$$

Histogram-based measures determine the degree of similarity between successive images not through the actual differences or correlations of intensity values but rather by their relative frequency. The normalized histogram of differences \mathcal{H} can also be thought of as the probability for a certain intensity difference $g \in [-G; G] \in Z$ with G being the largest possible grey value in the intensity image and $\delta(x, y)$ the Kronecker delta function (see also Ref. 11).

$$\mathcal{H}(g) = \frac{1}{N} \sum_{x_A \in \Omega_{A,B}^T} \delta(A(x_A) - B^T(x_A), g) \quad (15)$$

Shannon-Wiener developed a measure as part of a communication theory in the 1940s, which is called entropy (H, eq. 16) and which is based on the probabilities of random variables. H can also be used in image processing to measure the relative frequency of differences leading to the entropy of the histogram of differences (HHD, eq. 17) that has to be minimized. Meijering¹¹ stated that another measure, the energy of the histogram of differences (EHD, eq. 18) performs comparably to HHD at reduced computational costs.

$$H = - \sum_i p_i \log p_i \quad (16)$$

$$HHD = - \sum_{g=-G}^g \mathcal{H}(g) \log \mathcal{H}(g) \quad (17)$$

$$EHD = \sum_{g=-G}^g \mathcal{H}^2(g) \quad (18)$$

If image registration is regarded as the maximization of the amount of shared information that is given in two images, it can also be thought of as trying to reduce the quantity of information contained in the combined image. If two images are aligned correctly, corresponding structures will overlap and the information of the fusion image is minimal, whereas in the non-aligned case, duplicates of anatomic structures will result in an increased amount of information, as if two noses are present in the combined image. The Shannon-Wiener entropy, presented in eq. 16, is a commonly used metric in signal and image processing and can be used to express the amount of uniformity of random variables with given probabilities p_1, p_2, \dots, p_i . In the case of image registration, the information that is contributed to the overlapping volume by each image, as well as the joint entropy, i.e. the amount of information of the images combined, can be expressed by entropies. The joint entropy $H(A, B)$ of the images is minimal, if images A and B are most similar.

$$H(A) = - \sum_a p_A^T(a) \log p_A^T(a) \quad (19)$$

$$H(B) = - \sum_b p_B^T(b) \log p_B^T(b) \quad (20)$$

$$H(A, B) = - \sum_a \sum_b p_{AB}^T(a, b) \log p_{AB}^T(a, b) \quad (21)$$

A major drawback of $H(A, B)$ as a measure itself is its strong dependency on \mathcal{T} and the overlap domain Ω . For instance, the measure could tend to maximize the overlapping of large structures of similar intensity values and therefore lead to erroneous results if the starting point for the registration is poorly chosen. The solution is provided by an approach that also considers the information which is contributed to the registration by each of the images. It can be expressed by the entropies $H(A)$ and $H(B)$ (eq. 19, 20), where p_A^T and p_B^T are the marginal probability distributions of image A and the transformed and interpolated image B , respectively. The measure that takes the altering marginal probabilities into consideration with respect to the current transform is known as mutual information (MI, eq. 22) which can also be expressed in terms of the Kullback-Leibler distance (see Wells et al.¹² and Collignon et al.¹³). The MI is maximal for a transform \mathcal{T} that makes image A the best possible predictor for image B^T within the overlap domain. It can be used for intra- as well as for inter-modality registration but does not entirely solve the overlap problem. Studholme et al.¹⁴ proposed the usage of a normalized version, which is accordingly called normalized mutual information (NMI, eq. 23) and is considered to be more robust than the standard MI with respect to Ω .

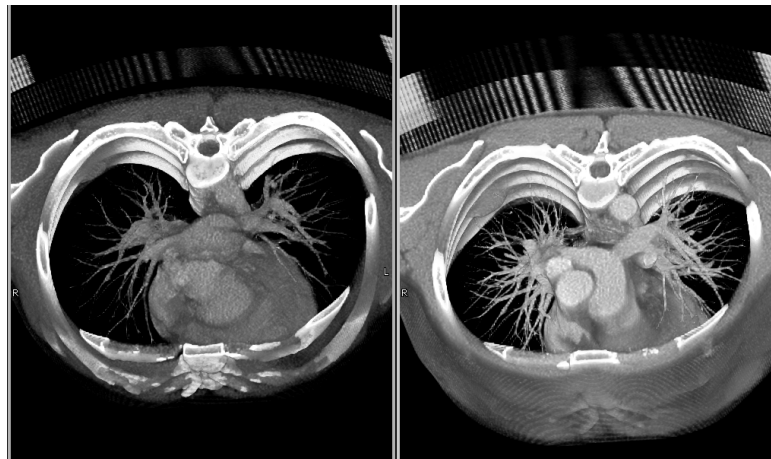
$$MI(A, B) = H(A) + H(B) - H(A, B) \quad (22)$$

$$NMI(A, B) = \frac{H(A) + H(B)}{H(A, B)} \quad (23)$$

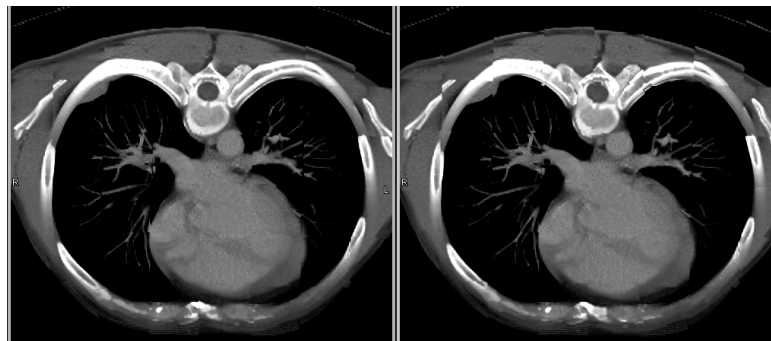
REFERENCES

1. L. G. Brown, "A survey of image registration techniques," *ACM Comput. Surv.* **24**(4), pp. 325–376, 1992.
2. P. V. D. Elsen, J. B. A. Maintz, E. Pol, and M. A. Viergever, "Medical image matching - a review with classification," *IEEE Engineering in Medicine and Biology* **12**(4), pp. 26–39, 1993.
3. D. L. G. Hill and P. G. Batchelor and M. Holden and D. J. Hawkes, "Medical image registration," *Physics in Medicine and Biology* **46**(3), pp. R1–R45, 2001.
4. J. Hajnal, D. Hill, and D. Hawkes, *Medical Image Registration*, CRC Press, 2001.
5. J. Maintz and M. Viergever, "A survey of medical image registration," *Medical Image Analysis* **2**(1), pp. 1–36, 1998.
6. R. P. Woods, S. T. Grafton, C. J. Holmes, S. R. Cherry, and J. C. Mazziotta, "Automated image registration: I. general methods and intrasubject, intramodality validation," *J. Comput. Assist. Tomogr.* **22**(1), pp. 139–152, 1998.

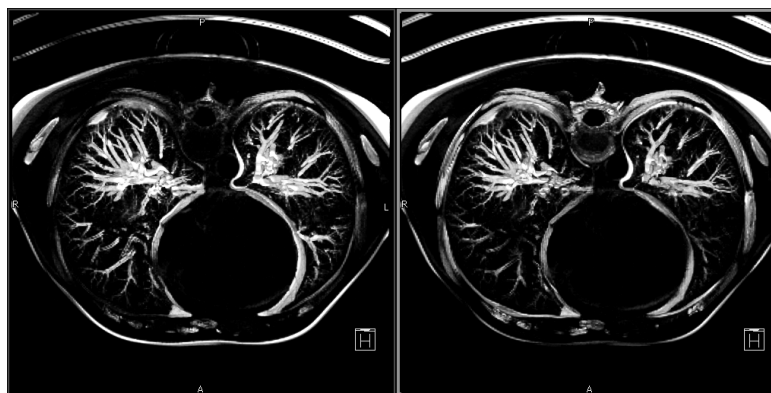
7. R. J. Althof and M. G. J. Wind and J. T. Dobbins, "A rapid and automatic image registration algorithm with subpixel accuracy," *IEEE Trans. Med. Imag.* **16**(3), pp. 308–316, 1997.
8. P. Venkataraman, *Applied Optimization with Matlab Programming*, ch. Numerical Techniques for Unconstrained Optimization. John Wiley and Sons Inc., 2002.
9. L. Armijo, "Minimization of functions having lipschitz continuous first-partial derivatives," *Pacific Journal of Mathematics* **16**(1), pp. 1–3, 1966.
10. *Inside InSpace from Siemens Medical Solutions and HipGraphics, Inc.*, 2004. <http://www.insideinspace.com>.
11. E. H. W. Meijering, *Image Enhancement in Digital X-Ray Angiography*. PhD thesis, Utrecht University, 2000.
12. W. Wells, P. Viola, H. Atsumi, S. Nakajima, and R. Kikinis, "Multi-modal volume registration by maximization of mutual information," *Medical Image Analysis* **1**(1), pp. 35–51, 1996.
13. A. Collignon, F. Maes, D. Delaere, D. Vandermeulen, P. Suetens, and G. Marchal, *Information Processing in Medical Imaging*, ch. Automated Multi-modality Image Registration Based On Information Theory, pp. 263–274. Kluwer Academic, Dordrecht, 1995.
14. C. Studholme, D. L. G. Hill, and D. J. Hawkes, "An overlap invariant entropy measure of 3D medical image alignment," *Pattern Recognition* **32**(1), pp. 71–86, 1999.



(a)



(b)



(c)

Figure 4. Fig. 4(a) shows a patient suffering from a tumor at the right dorsal thorax. The different registration methods lead to the CFIs in fig. 4(b) with the result of the proposed method in the left frame. Obviously, the motion of the lung and the heart cannot be addressed by a rigid transform, however, as an appropriate transfer function is applied (left of fig. 4(c)), the region of the tumor can be registered more precisely.

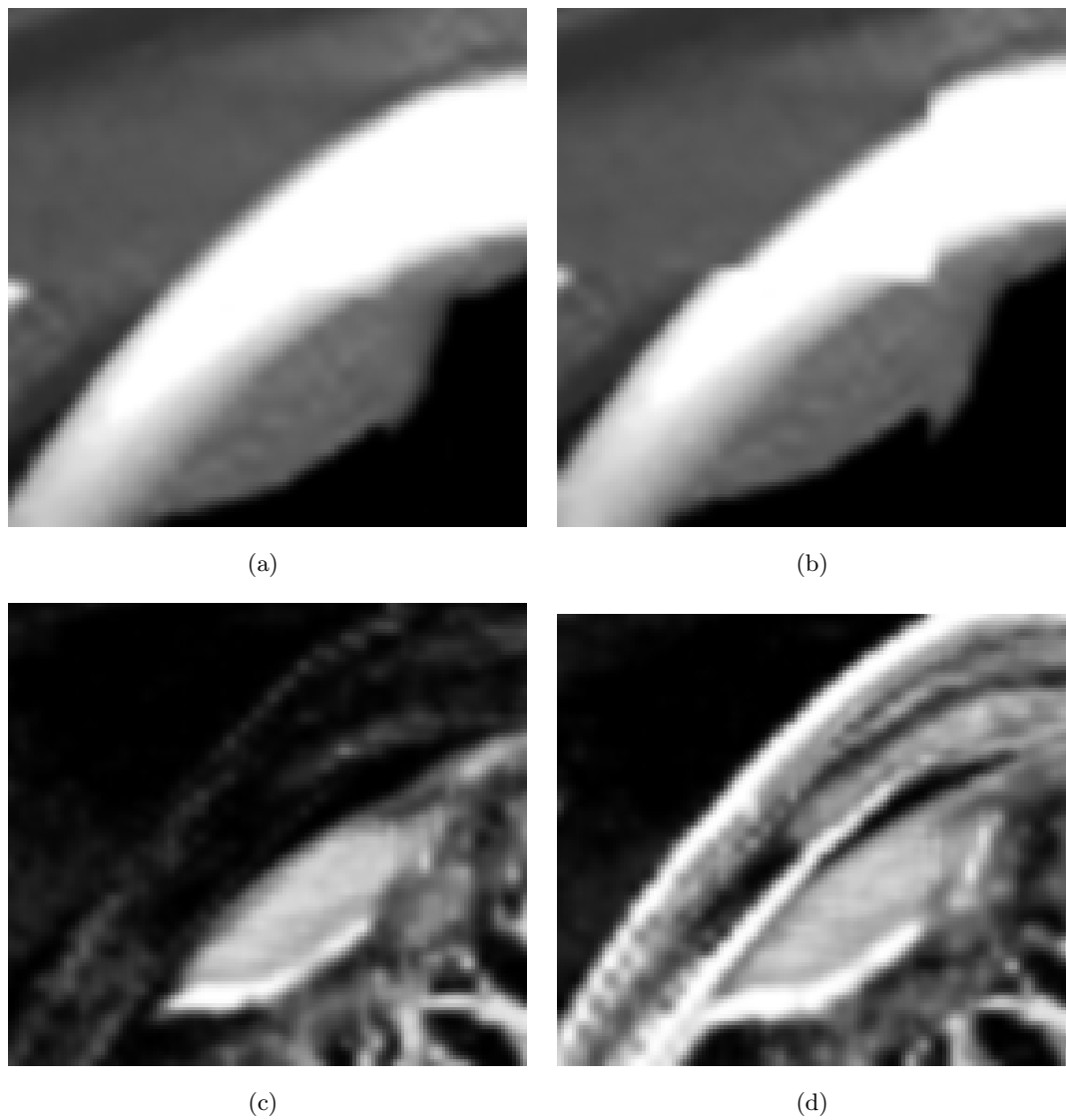
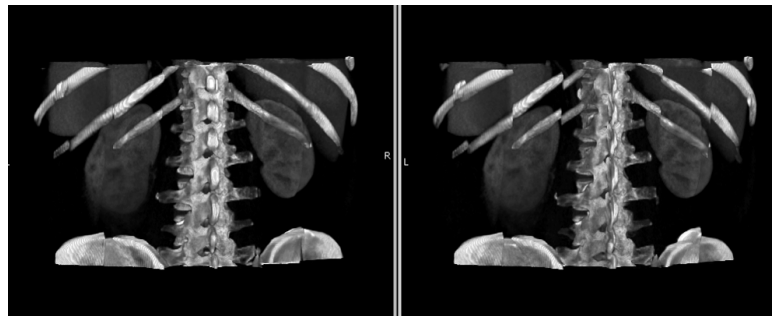
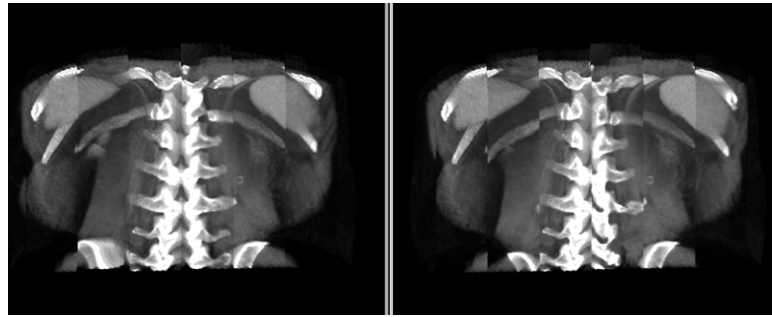


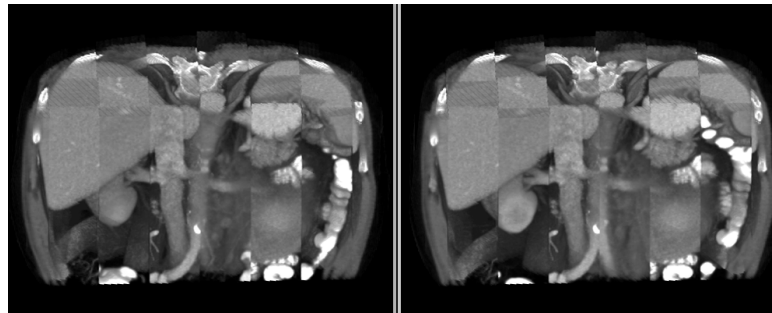
Figure 5. Zoom into the CFIs and difference volumes of lung tumor registration result of fig. 4. Fig. 5(a) shows the better alignment as a result of the proposed approach in comparison to the rigid registration using all voxel intensities (5(b)). Therefore, the difference image in fig. 5(c) features better information than the difference image using the common registration approach in fig. 5(d).



(a)



(b)



(c)

Figure 6. Alongside views of the 3D CFIs: the left CFIs result from the unbiased rigid registration with an appropriate transfer function applied on the registration, the right ones from from the common approach. Figures 6(a), 6(b) and 6(c) show different views on the same fused data set but with different transfer functions for the visualization (not used for the registration). The misalignment of the anatomical structures in the right images are clearly visible at the boundaries of the checkers.